Electronic Supplementary Material (ESI) for Journal of Analytical Atomic Spectrometry

Electronic supplementary information

Optimization of sample preparation and quadrupole ICP-MS measurement protocol for the determination of elemental impurities in pharmaceutical substances in compliance with USP guidelines

K. Van Hoecke[a], C. Catry[b] and F. Vanhaecke[a]

[a]: Ghent University, Department of Analytical Chemistry, Krijgslaan 281 – S12, B-9000 Gent, Belgium

[b]: Janssen Pharmaceutica NV, Turnhoutseweg 30, B-2340 Beerse, Belgium

CCT gas flow rate optimization

The He/H_2 gas mixture flow rate was optimized using the "ratio method". For this purpose, a 20 µg.L^{-1} Co solution in 10 % (v/v) HNO_3 and a 20 µg.L^{-1} Co and Ge solution in 10 % (v/v) aqua regia were prepared. In the 10 % HNO_3 solution, the $^{59}Co^+$ signal and the background signal at a mass-to-charge ratio of 56 were monitored as a function of increasing He/H_2 gas flow rate in steps of 0.5 ml.min^{-1} in the range 0.5-8 ml.min^{-1}. In the 10 % aqua regia solution, the background signals on mass-to-charge ratios of 51, 52, 53, 55 and 75 and the $^{59}Co^+$ and $^{74}Ge^+$ analyte signals were measured as a function of He/H_2 gas flow rate. A list of important interfering ions and the analyte monitored during the optimization (either Co or Ge) are given in **Table ESI-1**. For each mass-to-charge ratio subject to interference, the background to $^{59}Co^+$ or $^{74}Ge^+$ signal was plotted as a function of the He/H_2 gas flow rate. The onset of the plateau in the curve was selected as an optimum gas flow rate for operation in the CCT mode, as the corresponding setting provided minimum background at a sufficiently high analyte sensitivity. It was checked whether it was possible to select a common optimum gas flow rate suited for all analytes suffering from spectral overlap.

Table ESI-1 - Overview of important polyatomic ions causing spectral interference (non-restrictive list)

m/z	Interference(s)	Analyte used in optimization
51	$^{35}Cl^{16}O^+$, $^{36}Ar^{15}N^+$	Co
52	$^{35}Cl^{17}O^+$, $^{36}Ar^{16}O^+$, $^{38}Ar^{14}N^+$, $^{40}Ar^{12}C^+$	Co
53	$^{37}Cl^{16}O^+$, $^{35}Cl^{18}O^+$, $^{36}Ar^{16}O^1H^+$, $^{40}Ar^{13}C^+$, $^{40}Ar^{12}CH^+$	Co
55	$^{40}Ar^{15}N^+$, $^{17}Cl^{18}O^+$, $^{38}Ar^{16}O^1H^+$	Co
56	$^{40}Ar^{16}O^+$	Co
75	$^{40}Ar^{35}Cl^+$, $^{38}Ar^{37}Cl^+$	Ge

The signal intensities of important interfering ions at mass-to-charge ratios of 51-53, 55, 56 and 75 rapidly decreased when the He/H_2 gas mixture was introduced into the collision-reaction cell. At a gas flow rate of 4 to 5 ml.min^{-1}, the background intensity fell below 100 counts/s. Although the analyte intensities of Co and Ge also decreased at gas flow rates ≥ 2 ml.min^{-1}, the background-to-signal ratio improved with the introduction of the gas. **Figure ESI-1** illustrates the background-to-signal ratio and the analyte intensity as a function of collision-reaction gas flow rate. For all masses monitored, the optimum gas flow rate was 4-5 ml.min^{-1}. Hence, it was concluded that adopting one gas flow rate setting for the measurement of all target nuclides in

CCT mode would result in sufficiently low limits of detection. The actual gas flow rate for analysis was optimized on a daily basis and varied between 4.5 and 5.1 ml.min^{-1}.

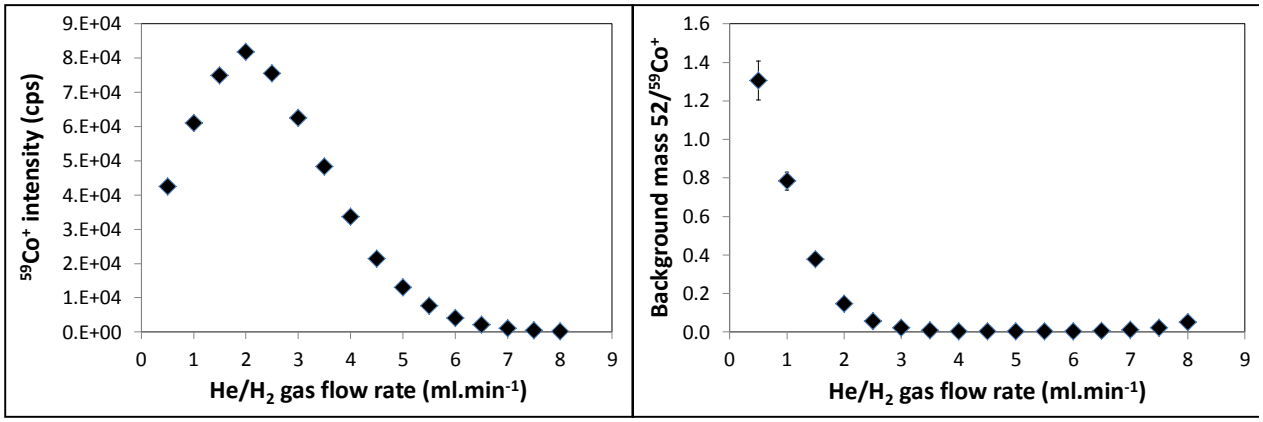

Figure ESI-1 - ^{59}Co$^+$ (20 µg.L^{-1}) analyte intensity (panel A) and ratio of background (at m/z = 52) to ^{59}Co$^+$ signal intensity (panel B) as a function of collision-reaction gas flow rate.

Two different mechanisms cause the efficient reduction of spectral interferences by polyatomic ions, *i.e.* collision and reaction. Yamada et al. (2002) demonstrated that polyatomic ions have lower kinetic energies compared to analyte ions at the exit slit of the collision-reaction cell as, due to their larger collisional cross-section, they collide more frequently with CCT gas molecules (ESI-1). The 3 V potential difference between the hexapole and the quadrupole acts as a kinetic energy filter that selectively removes the polyatomic ions with lower kinetic energy from the ion beam. Therefore, collisional deceleration in combination with kinetic energy discrimination efficiently reduces interferences from polyatomic ions. Second, the H_2 present in the CCT gas is reactive towards ArO^+, ArC^+, and $ArCl^+$ species (ESI2-3). Collision-induced reactions with H_2 cause neutralization and dissociation or modification of polyatomic species through charge transfer, proton transfer or hydrogen atom transfer reactions (ESI-4-5). However, H_2 is unreactive towards ClO^+. This means that only collision is involved in the elimination of the ClO^+ isobaric interferences affecting the determination of $^{51}V^+$, $^{52}Cr^+$, $^{53}Cr^+$ and $^{55}Mn^+$. However, as can be seen in **Figure ESI-2**, the background (at m/z = 51) to signal (at m/z = 59) can be sufficiently minimized for determination of V within the context of USP impurity determination. It is expected that a mixture of He/NH_3 would be more efficient to overcome ClO^+ interferences, as NH_3 can neutralize ClO^+. Chrastný et al. (2006) demonstrated that the use of He/NH_3 as

collision-reaction gas can improve the limits of detection with a factor of three compared to the He/H_2 collision-reaction gas (ESI-6).

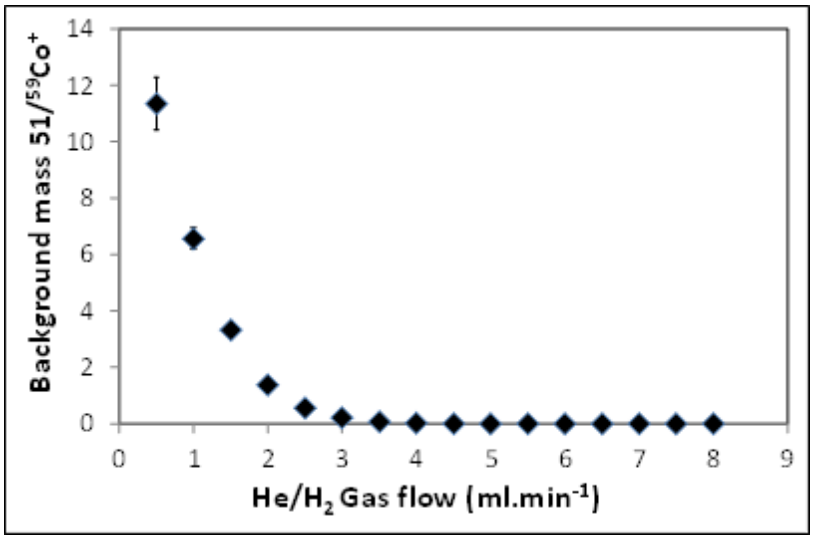

Figure ESI-2 - Ratio of background (at m/z = 51) to $^{59}Co^{+}$ (20 µg.L^{-1}) signal intensity as a function of collision-reaction gas flow rate in order to optimize $^{51}V^{+}$ measurements.

Elemental impurity determination and recovery in samples prepared via direct dissolution in 1 % (v/v) HNO_3 without the addition of $KBrO_3$

Table ESI-2 – Overview of limits of detection (LOD), limits of quantification (LOQ), correlation coefficients of calibration curves, impurity concentrations and spike recoveries in 10 g.L^{-1} solutions of Neosorb in 1 % HNO_3.

Nuclide	LOD[b]	LOD[c]	LOQ[d]	LOQ[e]	R^2[f]	Conc.[g]	Conc.[h]	RSD[i]	Recovery	RSD
	µg.L^{-1}	µg.g^{-1}	µg.L^{-1}	µg.g^{-1}		µg.L^{-1}	µg.g^{-1}	%	%	%
^{51}V[a]	0.007	0.0007	0.02	0.002	1.0000	< LOQ			100.4	0.8
^{52}Cr[a]	0.006	0.0006	0.1	0.01	0.9997	< LOQ			100.3	1.5
^{53}Cr[a]	0.03	0.003	0.1	0.01	1.0000	< LOQ			102.2	2.6
^{55}Mn[a]	0.04	0.004	0.04	0.004	0.9986	0.040	0.004	41.8	100.2	1.1
^{56}Fe[a]	0.01	0.001	3	0.3	1.0000	< LOQ			101.7	1.3
^{60}Ni	0.01	0.001	0.1	0.01	0.9997	< LOQ			102.5	1.0
^{62}Ni	0.01	0.001	0.06	0.006	0.9997	< LOQ			102.6	0.8
^{63}Cu	0.060	0.0060	0.2	0.02	0.9998	< LOQ			102.4	0.9
^{64}Zn	10	1	40	4	0.5067	< LOQ			50.4	62.9
^{65}Cu	0.040	0.0040	0.2	0.02	0.9997	< LOQ			102.3	1.2
^{66}Zn	10	1	40	4	0.4962	< LOQ			53.3	60.7
^{68}Zn	10	1	40	4	0.4850	< LOQ			53.4	61.0
^{75}As[a]	0.007	0.0007	0.02	0.002	1.0000	< LOQ			105.7	3.6
^{95}Mo	0.002	0.0002	0.008	0.0008	0.9997	< LOQ			104.1	0.9
^{98}Mo	0.002	0.0002	0.005	0.0005	0.9998	< LOQ			104.0	0.8
^{99}Ru	0.003	0.0003	0.008	0.0008	0.9999	< LOQ			104.7	0.9
^{101}Ru	0.004	0.0004	0.01	0.001	0.9998	< LOQ			105.0	1.4
^{103}Rh	0.006	0.0006	0.02	0.002	0.9999	< LOQ			104.9	1.2
^{105}Pd	0.05	0.005	0.2	0.02	0.9874	< LOQ			84.1	9.1
^{108}Pd	0.06	0.006	0.2	0.02	0.9869	< LOQ			84.6	9.0
^{111}Cd	0.004	0.0004	0.01	0.001	0.9999	< LOQ			103.0	1.1
^{189}Os	0.004	0.0004	0.02	0.002	1.000	< LOQ			108.8	1.1
^{191}Ir	0.002	0.0002	0.006	0.0006	0.9998	< LOQ	0.009	3.9	104.2	1.1
^{192}Os	0.004	0.0004	0.01	0.001	1.000	< LOQ			109.2	1.5
^{193}Ir	0.002	0.0002	0.006	0.0006	0.9998	< LOQ	0.011	6.6	104.3	1.1
^{194}Pt	0.002	0.0002	0.02	0.002	0.9999	< LOQ			102.1	1.8
^{195}Pt	0.006	0.0006	0.02	0.002	1.0000	< LOQ			102.3	1.5
^{200}Hg	n.d.	n.d.	n.d.	n.d.	0.4540	n.d.	n.d.	n.d.	n.d.	n.d.
^{201}Hg	n.d.	n.d.	n.d.	n.d.	0.4540	n.d.	n.d.	n.d.	n.d.	n.d.
^{202}Hg	n.d.	n.d.	n.d.	n.d.	0.4540	n.d.	n.d.	n.d.	n.d.	n.d.
^{206}Pb	0.01	0.001	0.03	0.003	0.9998	< LOQ			104.7	1.4
^{207}Pb	0.01	0.001	0.03	0.003	0.9999	< LOQ			104.6	1.4
^{208}Pb	0.01	0.001	0.03	0.003	0.9999	< LOQ			105.3	1.3

a: Nuclide measured in CCT mode.

b: Limit of detection; determined as the ratio of 3.3 x the standard deviation on 6 blank solutions and the slope of the calibration curve, expressed as concentration in solution (µg.L^{-1}).

c: same as b, but concentration expressed as concentration in pharmaceutical product (µg.g^{-1}).

d: calculated as 3.3x the limit of detection, expressed as concentration in solution (µg.L^{-1}).

e: same as d, but concentration expressed as concentration in pharmaceutical product ($\mu g.g^{-1}$).
f: Pearson correlation coefficient of a linear regression fitted to measured standard intensities as a function of standard concentration
g: concentration measured in solution
h: concentration calculated in the pharmaceutical product
i: relative standard deviation

Optimization of analysis for samples prepared via microwave-assisted acid digestion using concentrated HNO_3

Table ESI-3 - Elemental spike recoveries (mean and relative standard deviation (RSD), (n = 3)) for 10 $g.L^{-1}$ solutions of Neosorb 70/70 B in 10 % HNO_3 + 0.009 mM $KBrO_3$ + 1 % HCl prepared after microwave-assisted acid digestion. Left: 0.009 mM $KBrO_3$ in 1 % HCl added before microwave digestion; Right: $KBrO_3$ in HCl added after digestion.

	Digestion with 0.009 mM $KBrO_3$ + 1 % HCl in vessel				Digestion without $KBrO_3$ in HCl in vessel			
	Ext. Std.		Std. add.		Ext. Std.		Std. add.	
Nuclide	mean	RSD	mean	RSD	mean	RSD	mean	RSD
	%	%	%	%	%	%	%	%
^{51}V	99.2	0.4	98	0.4	98.1	0.4	96.5	0.4
^{52}Cr	99.4	0.7	98.1	0.7	98.7	1.5	97.9	1.5
^{53}Cr	99.9	0.7	98.2	0.7	99.3	1.0	97.3	1
^{55}Mn	102.4	0.5	101.6	0.5	101.5	0.7	100.5	0.7
^{56}Fe	111.6	6.5	110.2	6.4	102.8	2.2	102.6	2.2
^{60}Ni	95.0	0.6	95.7	0.6	93.7	1.0	98.5	1
^{62}Ni	95.2	0.8	95.0	0.8	93.7	1.2	98.1	1.2
^{63}Cu	97.7	0.5	97.2	0.5	96.5	1.0	101.3	1.0
^{64}Zn	85.0	4.0	89.4	4.1	87.0	8.7	94.6	8.7
^{65}Cu	97.5	0.3	97.4	0.3	96.2	1.0	101.3	1.0
^{66}Zn	84.8	4.1	89.3	4.2	86.8	9.0	94.4	8.9
^{68}Zn	84.8	4.4	89.2	4.5	86.9	9.0	94.4	8.9
^{75}As	109.2	1.7	98.5	1.7	98.0	4.0	92.5	3.9
^{95}Mo	97.3	0.5	96.9	0.5	96.6	0.7	96.9	0.7
^{98}Mo	97.2	0.5	97.3	0.5	96.6	0.7	97.0	0.7
^{99}Ru	98.8	0.7	98.9	0.7	98.0	0.8	98.4	0.8
^{101}Ru	98.8	0.4	98.9	0.4	98.1	0.8	98.6	0.8
^{103}Rh	97.1	0.3	97.8	0.3	96.8	0.5	98.1	0.5
^{105}Pd	84.4	11.5	86.9	11.3	74.4	15.6	80.7	15.2
^{108}Pd	85.6	11.2	86.7	11.2	75.2	14.9	80.5	14.7
^{111}Cd	91.4	0.8	95.4	0.8	91.1	0.8	100	0.8
^{189}Os	501.6	1.7	1033.7	1.6	487.8	5.1	1033.4	4.9
^{191}Ir	93.9	0.3	96.2	0.3	93.9	0.4	98.3	0.4
^{192}Os	503.7	1.3	1034.2	1.3	489.6	5.3	1031.5	5.1
^{193}Ir	93.9	0.2	96.1	0.2	93.8	0.2	98.6	0.2
^{194}Pt	89.4	0.5	92.4	0.5	89.7	0.7	97.9	0.7

^{195}Pt	89.5	0.5	92.4	0.5	89.8	0.5	97.7	0.5
^{200}Hg	83.5	1.1	90.5	1.0	87.9	1.3	98.3	1.3
^{201}Hg	77.7	0.3	90.2	0.3	80.7	1	97.1	1.0
^{202}Hg	86.0	0.4	92.6	0.4	89.1	0.7	98.7	0.7
^{206}Pb	112.5	0.7	107.3	0.8	107.1	0.5	105.4	0.5
^{207}Pb	104.2	0.8	97.3	0.8	99.6	0.4	96.2	0.4
^{208}Pb	110.8	0.3	104.5	0.3	105.4	0.3	103.2	0.3

References

ESI-1.Yamada, N., Takahashi, J., Sakata, K., 2002. The effects of cell-gas impurities and kinetic energy discrimination in an octopole collision cell ICP-MS under non-thermalized conditions. *J. Anal. At. Spectrom.*, 17, 1213–1222.

ESI-2. Feldmann, I., Jakubowski, N., Stuewer, D., 1999. Application of a hexapole collision and reaction cell in ICP-MS Part I: Instrumental aspects and operational optimization. *Fresenius J. Anal. Chem.*, 365, 415–421.

ESI-3. Stürup, S., Hayes, R. B., Peters, U., 2005. Development and application of a simple routine method for the determination of selenium in serum by octopole reaction system ICPMS. *Anal. Bioanal. Chem.*, 381, 686–694.

ESI-4. Koyanagi, G. K., Baranov, V. I., Tanner, S. D., Bohme, D. K., 2000. An inductively coupled plasma/selected-ion flow tube mass spectrometric study of the chemical resolution of isobaric interferences. *J. Anal. At. Spectrom.*, 15, 1207-1210.

ESI-5. Koyanagi, G. K., Lavrov, V. V., Baranov, V., Bandura, D., Tanner, S., McLaren, J. W., Bohme, D. K., 2000. A novel inductively coupled plasma/selected-ion flow tube mass

spectrometer for the study of reactions of atomic and atomic oxide ions. *Int. J. Mass Spectrom.* 194, L1–L5.

ESI-6. Chrastný, V., Komárek, M., Mihaljevič, M., Štíchová, J., 2006. Vanadium determination in chloride matrices using ICP-MS: finding the optimum collision/reaction cell parameters for suppressing polyatomic interferences. Anal. Bioanal. Chem., 385, 962–970.